Dyes and Pigments 211 (2023) 111050

Contents lists available at ScienceDirect

Dyes and Pigments

journal homepage: www.elsevier.com/locate/dyepig

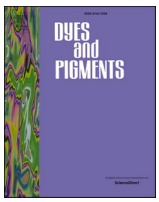

Tuning the colour of solution processed perylene tetraester based OLEDs from yellowish-green to greenish-white: A molecular engineering approach

Erkan Aksoy [a,b], Volkan Bozkus [b], Canan Varlikli [b,*]

[a] Project and Technology Office, Rectorate, Bartin University, 74100, Bartin, Turkey
[b] Department of Photonics, Izmir Institute of Technology, Urla, 35430, Izmir, Turkey

ARTICLE INFO

Keywords:
Regioisomericaly pure
Perylene
Solution processed
OLED
White light
Broad emission

ABSTRACT

Three regioisomericaly pure 1,7-di-ethynyl bridged perylene-3,4,9,10-tetracarboxy tetrabutylesters functionalized with triisopropylsilyl-ethynylen (PTE1), phenyl-ethynylen (PTE2) and tetraphenylsilyl-ethynylen (PTE3) groups were synthesized. Photophysical, thermal, electrochemical, and solution processed electroluminescence (EL) behaviours were investigated in comparison with a basic perylene-3,4,9,10-tetracarboxy tetrabutylester (PTEref) structure. Stepwise π conjugation, allowed tuning the absorption and photoluminescence wavelengths of the PTEs without disturbing the photo, thermal and electrochemical stabilities; ≫10h, >250 °C, and >50 cycles, respectively. Electron mobility of PTE2 is measured to be more than 10-fold of the other PTE derivatives. Individual utilization of PTE derivatives as solid-state emitters in poly(N-vinylcarbazole) (PVK): 2-(4-Biphenylyl)-5-phenyl-1,3,4-oxadiazole (PBD) host matrix produced yellowish-green EL. Benefiting from higher electron mobiliy, PTE2 emitter presented the best device efficiency values with an EL maximum of 535 nm. Whereas dual doping of the synthesized PTEs with PTEref resulted in greenish-white light with increased stability. Although the emitting layer contained no red emitting component, optimization of the dual doping ratio of PTEref:PTE3 produced a colour rendering index value of 76 with Commission Internationale d'Eclairage coordinates of (0.29, 0.37).

1. Introduction

The most well-known perylene derivatives are perylene diimides (PDIs) and perylene tetraesters (PTEs). Due to their high photoluminescence quantum yields (PLQYs) in the visible range, excellent electrochemical, photo, and thermal stability, they have attracted attention in molecular photonic technologies such as organic or perovskite solar cells, organic light emitting diodes (OLEDs), light emitting transistor displays and hybrid white LEDs [1–28].

Although planar PDIs suffer from low solubility in common organic solvents, and this restriction is relatively low for the PTEs, both PDI and PTE derivatives lose most of their PLQY due to dimer/aggregation formations in the film phase [19]. Therefore, especially in hybrid white LEDs, they are generally doped into optically inert polymers with very low mass ratios and to reach high colour rendering index (CRI) values, multiple layers of orange-red and green emitting PDI and/or PTE coatings become necessary [20,21].

The photoluminescence (PL) of PDIs is limited to orange-red and red regions, while emissions of PTEs can cover a wide range from blue-green to red. Non-functionalized PTEs have high band gaps due to their weak electron withdrawing esters, and exhibit blue-green PL in solution [21,29]. The most practical strategy to follow to shift the PL of PTEs towards the red region is to extend the π conjugation of the perylene core by electron donor groups. However, the application of this strategy results in low PLQYs even in solution phases [30]. On the other hand, curing the main PTE core with electron acceptor groups that contribute to the π conjugation not only allows the PL of the molecule to shift to longer wavelengths but also protects their PLQYs to some extent [31]. This situation increases the utilization potential of PTEs as emitters in single layer solution processed white OLEDs.

White light is obtained using primary (blue and orange) or complementary (red, green, blue- RGB) colours. The use of primary colours, which is widely used in the lighting industry, suffers from CRI values due to the absence of green region. Although using complementary colours is a remedy for this situation, in the case of narrow emission spectra, there will be spectral gaps between blue-green and green-red regions; cyan and yellow would be the missing regions [32,33]. Like most of the organic semiconductors, PTEs provide advantages with their wide

* Corresponding author.
E-mail address: cananvarlikli@iyte.edu.tr (C. Varlikli).

https://doi.org/10.1016/j.dyepig.2022.111050
Received 30 July 2022; Received in revised form 17 December 2022; Accepted 27 December 2022
Available online 28 December 2022

emission spectra [34].

In this study, a series of ethynyl bridged PTE derivatives with high PLQY, and optical-thermal-electrochemical stability were synthesized and their photophysical properties were investigated (Fig. 1). With the ethynyl, phenylethynyl and silanephenylethynyl groups modified PTEs, the conjugation was increased stepwise, and the band gap was narrowed; alternative emitters for green and green yellow regions were presented. Using synthesized PTEs as emitters in solution processed single layer OLEDs resulted in yellowish-green to greenish-white emission.

2. Experimental methods

2.1. Synthesis of PTE derivatives and characterization

The process known in the literature was repeated during the synthesis of regioisomericaly pure 1,7-dibromo PTE, PTEref, and ethynyl bridged TPhSi [35–37]. The ethynyl sources required for PTE1 and PTE2 were purchased and used in Sonogashira reactions. A summary of the synthetic steps were represented below, and structural characterization spectra were provided in Supplementary Information (SI).

2.1.1. Synthesis of 4-bromophenyl-triphenylsilane (mBr-TPhSi)

Freshly dried THF (desilted with sodium and benzophenone indicator) and 10 g of 1,4-dibromobenzene were transferred to a 250 mL 2-necked flask pre-heated under vacuum and Ar was introduced into the reaction system. The reaction flask was placed in a dry ice-acetone mixture, and after stirring for 20 min, 16.9 mL of n-butyl lithium (nBuLi) was added dropwise into the flask. After stirring for 90 min, chloro-triphenylsilane was added and stirred for 1 h at −78 °C (dry ice/acetone). Finally, the reaction was continued at room temperature for a night and terminated by adding 10 mL of 1 M HCl (aq) to the reaction medium. The reaction mixture was poured into purified water and extracted with chloroform (four times x 100 mL). The organic phase was evaporated, and some of the solid was purified by column chromatography (SiO_2: hexane). FTIR (KBr), ϑ_{max} (cm^{-1}) (Fig. S1): 3063 (C_{Ar-H}), 3007 (C_{Ar-H}), 1425, 1107, 748, 727, 696 cm^{-1}. ^1H NMR (400 MHz, $CDCl_3$, TMS/ppm) δ: 7.57–7.52 (m, 8H, Ar); 7.47–7.37 (m, 11H, Ar) (Fig. S2).

2.1.2. Synthesis of trimethyl-4-triphenylsilylphenylethynylsilane (TMSiA-TPhSi)

1.68 g of mBrTPhSi, 15 mL of toluene, and 30 mL of di(triisopropyl) amine was added to the 2-necked flask, and the reaction was stirred under Ar atmosphere. Then, 0.46 g Pd^0 and 0.07 g CuI and 0.7 mL of ethynyltrimethylsilane were added, the reaction was continued for 3 days at RT and terminated. The resulting solid was purified by column chromatography (SiO_2: hexane) after evaporation of the reaction solvent on a rotary evaporator. FTIR (KBr), ϑ_{max} (cm^{-1}): 3064 (C_{Ar-H}), 3015 (C_{Ar-H}), 2956, 2900 ($C_{Alkyl-H}$), 2161, 1591, 1425, 1105, 748, 727, 696 cm^{-1} (Fig. S3). ^1H NMR (400 MHz, $CDCl_3$, TMS/ppm) δ:7.56–7.36 (m, 19H, Ar); 0.26 (s, 9H) (Fig. S4). ^{13}C NMR (100 MHz, $CDCl_3$, TMS/ppm) δ: 136.34, 136.11, 135.12, 133.80, 131.13, 129.70, 127.92, 124.27, 105.05, 95.37, 0.06 (Fig. S5).

2.1.3. Synthesis of 4-(triphenylsilyl)-phenylacetylene (A-TPhSi)

50 mL of methanol and 0.43g of K_2CO_3 were added to the single necked flask and mixed for 10 min. Then, TMSiA-TPhSi was added to it and stirred at RT for 4 h. The reaction was terminated by decanting into pure water. Precipitated material was filtered and dried. Yield 84%. ^1H NMR (400 MHz, $CDCl_3$, TMS/ppm) δ: 7.56–7.36 (m, 19H, Ar); 3.13 (s, 1H, C≡C–H) (Fig. S6).

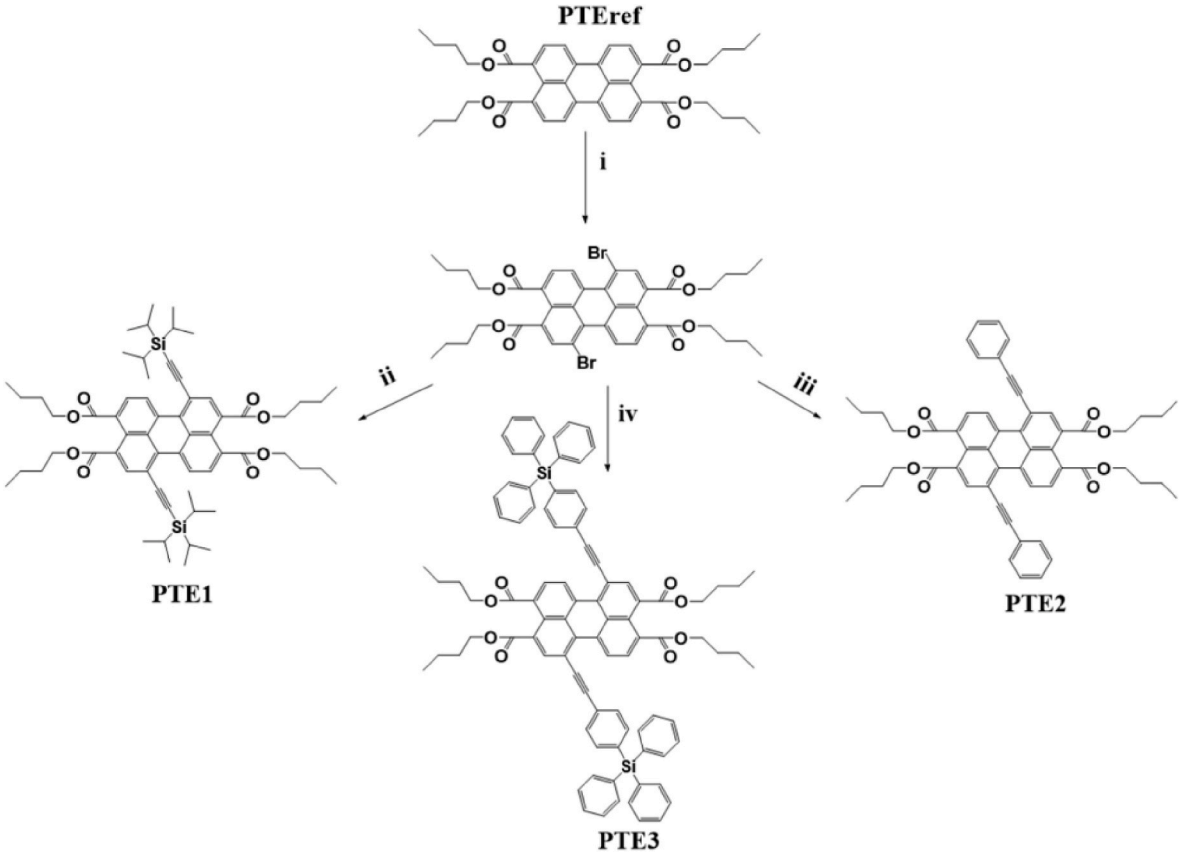

Fig. 1. Reaction scheme and molecular structures of PTEref, PTE1, PTE2, and PTE3. i) Bromination reaction of PTEref, ii, iii, and iv) Sonogashira reaction of dibrominated PTE with ethynyl bridged structures.

2.1.4. Synthesis of 1,7-di-(triisopropylsilane)ethynyl-perylene-3,4,9,10-tetracarboxy tetrabutylester (PTE1)

After adding 0.84 g of 1.7-DiBrPTE [36], 15 mL of diisopropylamine, 19 mg of CuI, and 115 mg of Pd(0) catalyst into the 2-necked flask, a vacuum atmosphere was provided. 2.3 mL of triisopropylethynyl was added to the reaction medium, stirred for 10 min at RT, and the reaction was terminated by monitoring by TLC. After evaporation of the organic solvent, the solid was purified by column chromatography. Yield; 22%. (Solubility in Solvent: ~70 mg/mL chloroform and toluene.) FTIR (ATR) ϑ_{max} (cm^{-1}): 2953, 2943, 2864 (aromatic and aliphatic C–H Stretching), 2129 (alkyne), 1732 and 1712 (ester carbonyl) (Fig. S7).^{1}H NMR (400 MHz, chloroform-d, TMS/ppm) (Fig. S7): 9.71–9.69 (d, J:8Hz, 2H), 8.21 (s, 2H), 8.04–8.02 (d, J:8Hz, 2H), 4.34 [(td, 8H), 1.77 (m, 8H), 1.48 (m, 8H), 1.19 (m, 42H total), 0.99 (t, 12H) (Fig. S8). ^{13}C NMR (100 MHz, chloroform-d, TMS/ppm) δ (Fig. S9):168.21, 167.88, 136.94, 133.61, 132.28, 130.37, 130.00, 129.88, 129.38, 127.13, 127.07, 118.14, 107.79, 99.90, 65.49, 65.30, 30.56, 30.52, 19.25, 19.21, 18.74, 13.78, 11.36.

2.1.5. Synthesis of 1,7-di-phenylethynyl-perylene-3,4,9,10-tetracarboxy tetrabutylester (PTE2)

After adding 200 mg (2.47×10^{-4} mol) of 1,7-dibromoPTE, 10 mL of diisopropylamine, and 10 mL of toluene to the reaction flask the mixture was stirred under atmospheric conditions for 10 min. Then 4.7 mg (2.47×10^{-5} mol) CuI and 16 mg (2.47×10^{-5} mol) $Pd(Cl_2)(PPh_3)_2$ was added and stirring was continued for another 10 min. Finally, 270 μL (2.47×10^{-3} mol) of phenylacetylene was added and was kept at RT for 3 days. After the reaction solvent was evaporated, it was purified by column chromatography [SiO_2, chloroform: hexane (3:1)]. Yield; 84%. Solubility in Solvent: ~40 mg/mL chloroform and ~20 mg/mL toluene. FTIR (ATR) ϑ_{max} (cm^{-1}) (Fig. S7): 2957, 2931, 2872 (aromatic and aliphatic C–H Stretching), 2193 (alkyne), 1703 (ester carbonyl). ^{1}H NMR PTE2 (400 MHz, chloroform-d, TMS/ppm) δ (Fig. S10): 9.55–9.53 (d, J:8, 2H), 8.31 (s, 2H), 8.16–8.14 (d, J:8, 2H), 7.63–7.61/7.62–7.60 (dd, J:8Hz, 4H), 7.43 (m, 6H), 4.38–4.33 (q, J:8Hz, 8H), 1.78 (m, 8H), 1.49 (m, 8H), 1.02–0.97 (q, 8Hz 12H). ^{13}C NMR PTE2 (100 MHz, chloroform-d, TMS/ppm) δ (Fig. S11):168.32, 167.94, 135.93, 133.48, 132.43, 131.79, 129.11, 128.64, 126.78, 122.67, 118.11, 95.43, 90.78, 65.61, 30.63, 30.58, 19.28, 13.82.

2.1.6. Synthesis of 1,7-di-[(4-ethynylphenyl)(triphenyl)silyl]-perylene-3,4,9,10-tetracarboxy tetrabutylester (PTE3)

The reaction conditions used for PTE1 were used in the synthesis of PTE3. In this reaction, 0.1g of 1.7-DiBrPTE, 5 mL of diisopropylamine, 1.7 mg of CuI, 8 mg of Pd0 and 74 mg of TPhSiA were used. The reaction was terminated after monitoring by TLC. After the reaction solvent was removed by a rotary evaporator, the solid was purified by column chromatography (SiO_2: chloroform: hexane, 1:1). Yield; 79%. Solubility in solvent: ~40 mg/mL chloroform and ~20 mg/mL toluene. FTIR (ATR) ϑ_{max} (cm^{-1}) (Fig. S7): 2957, 2920, 2872 (aromatic and aliphatic C–H Stretching), 2193 (alkyne), 1709 (ester carbonyl). ^{1}H NMR (400 MHz, chloroform-d, TMS/ppm) (Fig. S12): 9.54–9.52 (d, J:8Hz, 2H), 8.30 (S, 2H), 8.15–8.13 (d, 8Hz, 2H), 7.65–7.59 (m, 20H total), 7.43–7.30 (m, 18H total), 4.36 (q, 8H), 1.79 (m, 8H), 1.14 (m, 8H), 0.99 (t, 6H), 0.96 (t, 6H). ^{13}C NMR (100 MHz, chloroform-d, TMS/ppm) δ (Fig. S13): 168.29, 167.93, 136.37, 136.48, 136.15, 133.59, 129.82, 128.02, 127.23, 124.06, 123.75, 123.50, 118.02, 95.41, 91.72, 65.63, 31.62, 30.56, 29.64, 19.22, 13.81.

2.2. Device fabrication and characterization

Indium tin oxide (ITO) glass substrates were patterned by HCl etching, cleaned by following the general methods [22,23], and then O_2 plasma treatment was applied for 8 min at 70 W. Poly(3, 4-ethylenedioxythiophene)-poly(styrenesulfonate) (PEDOT:PSS) was filtered twice with RC 0.45 μm filter, coated using spin coating system under atmospheric conditions for 1 min at 3000 rpm and annealed at 150 °C for 30 min. After the PEDOT:PSS coating, the substrates were transferred into an N_2 filled glove box system. Poly (N-vinylcarbazole) (PVK): 2-(4-biphenylyl)-5-phenyl-1,3,4-oxadiazole (PBD) (60:40 wt% in chlorobenzene, 30 mg/ml) was utilized as the host matrix for the synthesized PTE derivatives. Active layers of PVK:PBD:PTEX (0.1 wt%) (X = ref, 1, 2, and 3), PVK:PBD:PTEref:PTE1-3 (0.06:0.06 wt%) and PTEref: PTE3 (0.06:0.06, 0.03:0.06, 0.03:0.06, and 0.03:0.03 wt%) were spin coated under inert atmosphere for 1 min at 3000 rpm and annealed at 150 °C for 30 min. These active layers were labeled as the A, B, and C series, respectively. Cs_2CO_3 and Al were coated using physical thermal evaporation under 10^{-6} mbar with a deposition rate of 0.2 Å/s and 2 Å/s, respectively. Device labelling was done in accordance with the active layer label. D series devices contains 0.1 wt%:0.1 wt% and 0.2 wt %: 0.2 wt% of PTEref:PTEX (X:1, 2 or 3) in their active layer and named D1,D2, D3, D4, D5 and D6, respectively. Six parallel devices with structure of ITO/PEDOT:PSS(75 nm)/Active layer(85 nm)/Cs_2CO_3(2.3 nm)/Al(100 nm) and active area of 7 mm^2 were fabricated.

The energy diagram of the fabricated devices is provided in Fig. 2.

3. Result and discussion

3.1. Steady state absorption and photophysical properties of PTEs

UV–Vis absorption, PL, absolute PLQY, and lifetime (τ, ns) measurements were performed in both chloroform and film to determine the basic photophysical properties of PTEs. PTE1, PTE2, and PTE3 were functionalized with an ethynyl bridge from the −1 and −7 bay positions of PTEref. Active participation of these bridges in the π electron delocalization of the perylene core resulted in red shifts of the maximum absorption (λ_{abs}^{max}) and maximum PL (λ_{PL}^{max}) peaks of PTE; λ_{abs}^{max} shifts of 29 nm–46 nm and λ_{PL}^{max} shifts of 31 nm–59 nm were measured for PTE1-3 compared to the corresponding values of PTEref. PTE2 and PTE3 exhibited the highest λ_{abs}^{max} and λ_{PL}^{max} due to their further continued delocalization on the phenyl ring (Fig. 3 and Table 1). The extension of the delocalized conjugated π electron system with the addition of ethynyl and phenyl ethynyl substituents on the −1 and −7 bay positions of PTEref increased the Stokes shifts (Δλ, cm^{-1}) and reduced the self-absorption probability as well. However, it did not make a significant effect on the PLQY and τ values of PTEref; all of the synthesized derivatives exhibited general PTE properties of high PLQY (75.6%–94%) and short τ (5.6 ns–3.9 ns) [21,29,38] in chloroform (Table 1).

Film phase absorption and PL spectra of PTEref and PTE1, PTE2, and PTE3 are given in Figs. S14a–d λ_{abs}^{max} and λ_{PL}^{max} of PTEs in the film are 494 and 595 nm (PTEref), 502 and 583 nm (PTE1), 522 and 586 nm (PTE2), 532 and 626 nm (PTE3), respectively (Table 1). They all presented wider, red shifted absorption and PL spectra and reduced PLQY values compared to their solution behaviours. This situation was especially significant for PTEref and attributed to excimer or dimer/aggregate formations in the film [21,31]. However, the aggregation tendencies of the derivatives are thought to be quite different from each other [39] as the increment ratios ($\frac{\Delta\lambda film}{\Delta\lambda solution}$) detected in Δλ values were 4.0, 3.1, 1.2, and 2.5 for PTEref, PTE1, PTE2, and PTE3, respectively. Additionally, the lifetime (τ) of PTEref has increased while the others showed a decrement in the partial or direct curves (Table 1 and Fig. S15b). It was thought that although the addition of silylethynyl substituents increased the steric effects, they could not prevent aggregation but affected the aggregation types [39]. This situation would influence their electrochemical and electrical properties and consequently their PL and EL behaviours in optically inert hosts and OLEDs, respectively [20,21,40].

3.2. Electrochemical properties and stability behaviour of PTEs

Electrochemical characterizations of PTE1, PTE2, and PTE3 were carried out to investigate the effect of 1,7-di ethynyl group on reduction,

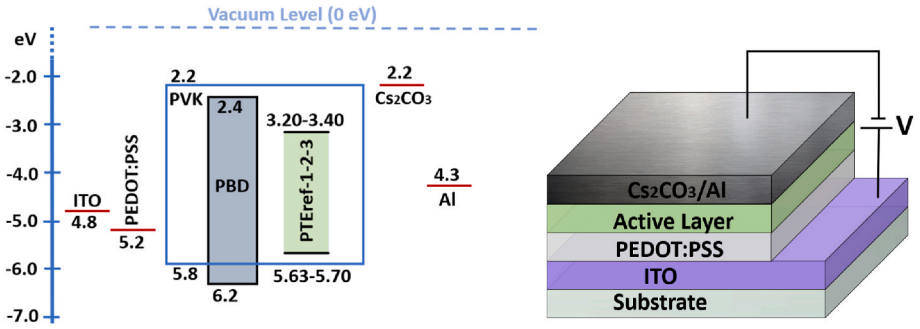

Fig. 2. Energy band diagram (left) and device structure (right) of fabricated OLEDs.

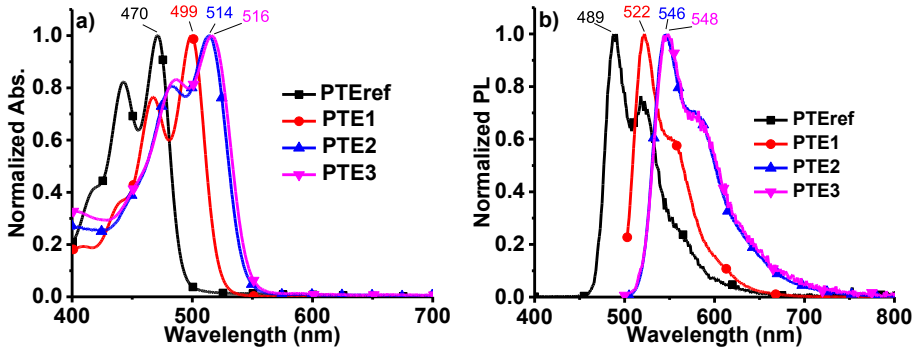

Fig. 3. a) Absorption and b) PL spectra of PTEref, PTE1, PTE2, and PTE3 in chloroform.

Table 1
Photophysical properties of PTEs in chloroform [1×10^{-6} M] and film [maximum absorption, λ_{abs}^{max} and maximum PL, λ_{PL}^{max} peaks (nm); Stokes shift, $\Delta\lambda$ (cm^{-1}); PLQY, (Φ%); lifetime, τ (ns); half-life, $t_{1/2}$ (h)].

PTEs	In solution						In film				
	λ_{abs}^{max}	λ_{PL}^{max}	$\Delta\lambda$	Φ%	τ	$t_{1/2}$	λ_{abs}	λ_{PL}^{max}	$\Delta\lambda$	Φ%	τ
ref	470	489	826	94.0	3.9	>10	494	595	3336	17.3	15.9
1	499	522	882	86.5	5.1	>10	502	583	2767	1.2	[a]
2	514	546	1140	98.0	5.6	>10	552	599	1421	2.8	[a]
3	516	548	1131	75.6	5.4	>10	532	626	2822	5.3	[a]

[a] Could not be detected due to fast decay (Fig. S15).

oxidation potentials, highest occupied molecular orbital (HOMO), and lowest unoccupied molecular orbital (LUMO) levels by using cyclic voltammetry measurements (Fig. 4 and Table 2). Although PTE derivatives exhibit a double reduction potential similar to PDIs [31], they also have oxidation peaks [41]. This generates weaker electron acceptor

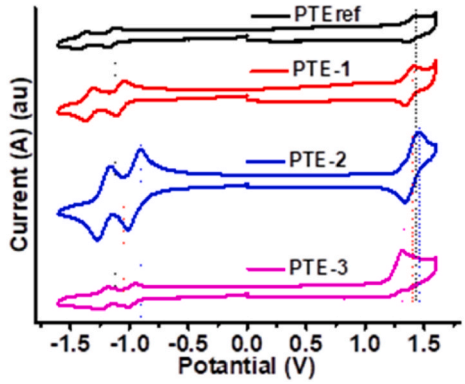

Fig. 4. Voltammogram curves of solutions of PTEref, PTE1, PTE2, and PTE3 with 0.1 M $TBAPF_6$ in DCM.

Table 2
Reduction, oxidation, optical band gap, HOMO and LUMO energy levels of PTEs.

PTEx	E_{Red} (V)	E_{Oxd} (V)	ΔE_{Opt} (eV)	HOMO (eV)	LUMO (eV)
Ref	−1.11/-1.40	1.40	2.50	−5.74	−3.24
1	−1.04/−1.34	1.37	2.36	−5.67	−3.31
2	−0.90/−1.20	1.39	2.26	−5.71	−3.45
3	−0.94/−1.22	1.26	2.26	−5.67	−3.41

property of ester groups compared to the imides of PDIs, which makes the perylene core of PTE more electron-rich [31]. The first reduction potential values of PTEs were −1.11, −1.04, −0.90, and −0.94 V, respectively. When the ethynyl groups were substituted to the 1,7-positions of PTE, this value was decreased by 0.07, 0.21 and 0.17 V, respectively, relative to PTEref. The LUMO energy levels of the PTEs were calculated using their first reduction potential and by utilizing the optical band gap calculated from the onset of the absorption spectrum, corresponding HOMO energy levels were extracted [42]. LUMO:HOMO energy levels of PTEref, PTE1, PTE2 and PTE3 are −3.24 eV: −5.74 eV, −3.31 eV: −5.67 eV, −3.45 eV: −5.71 eV and −3.41 eV: −5.67 eV, respectively. The decrements in the first reduction potentials and deeper LUMO energy levels of PTE1-3 suggested that they would be better electron acceptors and would present enhanced electron mobility (μ_{e-})

values compared to the PTEref.

To support this suggestion on the expected enhanced μ_{e-} and to better understand the effects of molecular structure of synthesized PTEs on OLED performance, μ_{e-} studies were carried out with a device structure of 'Al/PTEref or PTE1-3/Al' by using space charge limited current (SCLC) model at room temperature. The μ_{e-} values were found as 3.9×10^{-4} 2.3×10^{-4}, 2.0×10^{-2} and 2.7×10^{-3} $cm^2V^{-1}s^{-1}$, respectively (Fig. S16). The order of magnitude of the μ_{e-} values was the same as the LUMO energy levels.

Molecular models of the PTEref and PTE1-3 were computed, and 3D structures of the synthesized PTEs showed that their packaging in the film phase would be different (Table S1). The slightly increased μ_{e-} value of PTE1 compared to that of PTEref, was attributed to ethynyl bridged silane groups with tetrahedral geometry. Although PTE3 also contained silane groups with similar geometry, the TPhSi it contained has an extra phenyl group which increased the distance between the perylene core and substituent could not prevent the π- π stacking in the film phase as much as the free silane of PTE1. PTE2's 3D structure revealed that it was the most favorable structure for electron delocalization within the PTEs since it lacked tetrahedral geometry and, with its table plate like form, it was the most likely structure for π- π stacking (Table S1 and the videos of synthesized PTE derivatives).The obtained μ_{e-} values were in accordance with the literature as they have increased with decreased π- π stacking distance [17,18].

Continuous cyclic investigation of the PTEs in the range of +1.6 V to −1.6 V was made, and the 52nd measurements were taken by degassing with nitrogen gas. Comparison of their 1st and 52nd measurements addressed their high electrochemical stability (Fig. S17).

Photostability and thermal stability tests were also carried out. All PTEs were stimulated at their λ_{abs}^{max}, and the PL intensities (λ_{PL}^{max}) were monitored for 1 h by taking data per second. The time dependent PL intensities pointed out their great photostability (Fig. S18).

In thermal gravimetric analysis, the temperatures at which PTEs started to decompose were determined. The first mass losses were detected at 340 °C, 345 °C, 300 °C and 284 °C for PTEref, PTE1, PTE2, and PTE3, respectively (Fig. S19).

3.3. Yellowish-green to greenish-white electroluminescence

Synthesized PTEs were embedded in PVK:PBD host and used as n-type emitters in the active layer of 'ITO/PEDOT:PSS/Host:PTE/Cs_2CO_3/Al' device structure. Device characteristics of A (0.1 wt% PTEref, PTE1, 2 and 3, named as A_{ref}, A1, A2, and A3, respectively), B (PTEref:PTE1, PTEref:PTE2 and PTEref:PTE3 with 0.06:0.06 ratio, named as B1, B2 and B3, respectively) and C (PTEref:PTE3 rations of 0.06:0.06, 0.03:0.06, 0.03:0.06, and 0.03:0.03 named as C1, C2, C3, and C4, respectively) series devices containing different emitter combinations are given in Figs. S20–S24 and summarized in Tables 3–5.

The blue component observed in EL versus λ curves of the devices at 437 nm was generated from the host (Fig. 5) [22] and the shifts observed between 500 nm and 550 nm were consistent with the PL behaviours (Fig. 3b). Although the wavelength coverage of all devices was the same, the wavelength correspondences and intensities of the peaks were quite different. A1-3 devices presented the formation of a new peak at 470 nm (Fig. 5a). The probability of electroplex formation is eliminated with the voltage dependent EL measurements as the intensity of this peak did not change with the applied voltage (Fig. S21) [22,43]. It is thought that this peak should remain in B (Fig. 5b) and C (Fig. 5c) series devices and appear in the PL of films of active layers of A1-A3 (Fig. S22a) in case it was generating from the exciplex formation between the host and the PTEs. Further investigation on the nature of this peak was performed through lifetime measurements by collecting the luminesce decays at 470 nm (Fig. S22b) and excitation at 441 nm, where all the PTEs could, but the host could not be excited. The τ values of 43.4 ns, 5.1 ns, and 11.1 ns that has the same tendency with the increment ratios of Δλ of PTE1, PTE2 and PTE3 were obtained for the active layers of A1, A2 and A3 devices, respectively. This result corroborated that the peak at 470 nm could be attributed to different π-π stacking properties of PTE1-3 than that of PTEref as discussed above.

Luminance and maximum current efficiency values of A_{ref}, A1, A2 and A3 were measured as 233, 35, 442, 196 cd/m^2 and 0.23, 0.023, 0.436 and 0.184 cd/A, respectively. Although these values can be considered below the state of the art of greenish emitting OLED literature based on PTE derivatives [19,24–28], it is thought that they have a decent position with their vacuum thermal evaporated hole transfer, electron transfer and/or hole blocking layer free nature. Device A2 of PTE2, has the highest μ_{e-} exhibited the best efficiency values with the lowest turn on voltage of 8.2 V. The lowest full width of half maximum (FWHM) value was also obtained with the A2 device and suggested better energy transfer probability from the host to PTE2. However, regarding the potential to reach high CRI values with its FWHM value of 203 nm and integrated area of 181, device A3 was the best among the 'A' series devices (Fig. S20).

In B series devices, the increment of spectral coverage possibility with better device efficiency values is evaluated. Efficiency values were extracted from Fig. S23 and summarized in Table 4. Since the intensity of blue EL at 437 nm was decreased dramatically due to the increased amount of n-type semiconductors in the active layer, and 470 nm peak disappeared, spectral coverage was decreased compared to the A series (Fig. S24 versus Fig. S21). Nevertheless, the colour was shifted from green (A_{ref} device) to yellowish-green, and the efficiency values were increased. B3 is the best device of the B series with its high luminescence, high current efficiency, and wider FWHM compared to the others.

A broader EL spectrum can be obtained with the B3 device that contains PTE3. For this reason, a device optimization study, defined as C series, was carried out by changing the ratios of PTEref and PTE3. With the reduced perylene doping in C3 and C4 devices, the blue EL intensity of the host system was increased more than those of green and yellow region intensities (Fig. 5c and Fig. S25), and thus, an increase in CRI and CCT values was observed (Table 5). Even though these devices did not contain vacuum thermal evaporated electron transfer or hole blocking layers, their luminance and CCT values were comparable with the literature [26]. However, the decrease in the total amount of emitting material, PTE, resulted in a decrement of the efficiency values.

Lastly, increment of the doping ratios of PTEref:PTEX to 0.1:0.1 and 0.2:0.2 were employed in devices named as D series. Although luminance values of more than 1000 cd/m^2 could be obtained with some of these devices, CIE coordinates approached green. The charge balance detoriation increased the turn-on voltages and decreased the efficiency values (Table S2, Figs. S27–28).

Table 3
Luminance (cd/m^2), turn-on voltage (V), power efficiency (PE, lm/W), current efficiency (CE, cd/A), external quantum efficiency (EQE, %), full width of half maximum (FWHM, nm), colour rendering index (CRI) and Commission Internationale d'Eclairage coordinates (CIE, x,y) of A_{ref}, A1, A2, and A3 devices.

Device	Lum. (cd/m^2)	Turn-on (V)	PE (lm/W)	CE (cd/A)	EQE (%)	FWHM[a] (nm)	CRI	CIE (x,y)
A_{ref}	233	8.3	0.066	0.230	0.095	157	67	(0.28, 0.41)
A1	35	15.5	0.004	0.023	0.013	112	61	(0.37, 0.47)
A2	442	8.2	0.125	0.436	0.159	89	60	(0.37, 0.44)
A3	196	9.2	0.050	0.184	0.081	203	71	(0.32, 0.37)

[a] FWHM for the whole spectrum.

Table 4
Luminance (cd/m^2), turn-on voltage (V), power efficiency (PE, lm/W), current efficiency (CE, cd/A), external quantum efficiency (EQE, %), full width of half maximum (FWHM, nm), correlated colour temperature (CCT), colour rendering index (CRI) and Commission Internationale d'Eclairage coordinates (CIE, x,y) of B1-3.

Device	PTEref: X	Lum. (cd/m^2)	Turn-on (V)	PE (lm/W)	CE (cd/A)	EQE (%)	FWHM[a] (nm)	CCT (K)	CRI	CIE (x, y)
B1	PTE1	570	12	0.146	0.70	0.224	75	6005	58	(0.31, 050)
B2	PTE2	625	10.3	0.154	0.71	0.264	110	6228	61	(0.31, 0.45)
B3	PTE3	635	9.0	0.28	0.88	0.35	120	6195	67	(0.31, 0.44)

[a] FWHM for the whole spectrum.

Table 5
Luminance (cd/m^2), turn-on voltage (V), power efficiency (PE, lm/W), current efficiency (CE, cd/A), external quantum efficiency (EQE, %), full width of half maximum (FWHM, nm), correlated colour temperature (CCT), colour rendering index (CRI) and Commission Internationale d'Eclairage coordinates (CIE, x,y) of C1-4 devices (Values extracted from Fig. S26.).

Device	PTEref:PTE3 (wt%:wt%)	Lum. (cd/m^2)	Turn-on (V)	PE (lm/W)	CE (cd/A)	EQE (%)	CCT (K)	CRI	CIE (x,y)
C1=B3	0.06:0.06	635	9.0	0.28	0.88	0.35	6195	67	(0.31, 0.44)
C2	0.06:0.03	666	8.0	0.17	0.58	0.22	7159	62	(0.28, 0.42)
C3	0.03:0.06	422	8.2	0.14	0.45	0.20	7233	76	(0.29, 0.37)
C4	0.03:0.03	401	8.4	0.14	0.45	0.19	7710	71	(0.29, 0.38)

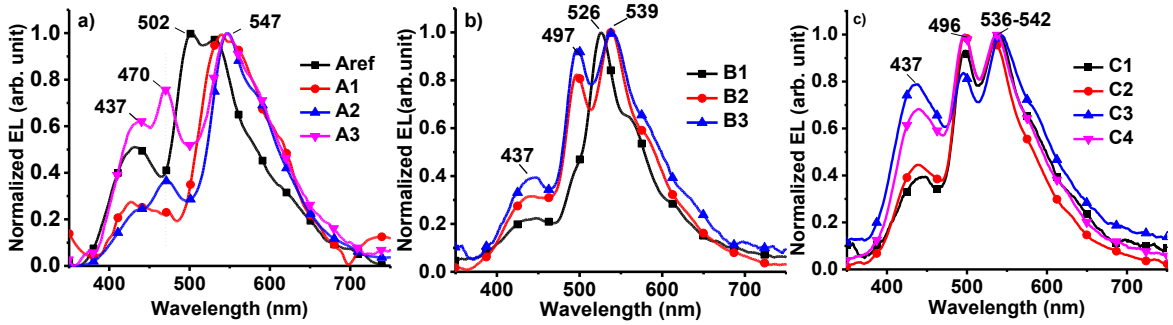

Fig. 5. Electroluminance characteristics of a) A_{ref}, A1-3, b) B1-3, and c) C1-4 devices.

In addition to CRI, colourability values, which is one of the extensively used measures in industry and shows the colour differences between the sample and D65, of the devices were also calculated. Mathematical expression of colourability [44] and CRI [45,46] were given in the SI as Eq.1 and Eq.2. The comparison of calculated colourability values of most of the devices with the highest CRI values (A3, B3 and D5) within the corresponding device series (Table S3), created the expectation that low colourability value would accompany high CRI. But this expectation did not apply either to the comparison of C3 and C4 devices, nor to the A3 and C4 devices. Although the CRI value of C3 (76) was higher than the C4 (71) the colourability was also higher (Table S3) and three-folds of difference was detected between the colourability values of A3 and C4 devices which have the same CRI values. This situation was attributed to the approach differences between these two widely used quantitative values; as the colourability is determined by the D65 [47], it considers CIE coordinates of (x, y; 0.3128, 0.329) while the CRI value is determined by the light source's spectrum.

4. Conclusion

λ_{abs}^{max} and λ_{PL}^{max} of PTEref and PTE1-3 were 470–489 nm, 499–522 nm, 514–546 nm, and 516–548 nm, respectively. PTEref, PTE1, and PTE2 exhibited high fluorescence quantum yields (PLQY≥85%) whereas PTE3 has a relatively moderate PLQY (~75%) due to the bulky nature of tetraphenylsilane structure. Fluorescence lifetimes of all PTEs were in the range of 3–6 ns and photo, thermal and electrochemical stabilities were >10h, ≥300 °C and >50 cycles, respectively. Electron mobility values of the synthesized derivatives varied between 2.0×10^{-2} $cm^2V^{-1}s^{-1}$ and 3.9×10^{-4}, continued delocalization of π electrons within the planar structure of PTE2 allowed reaching the highest electron mobility.

The PTE derivatives were utilized as solid-state emitters in the solution processed active layer (AL) of ITO/PEDOT:PSS/AL/Cs_2CO_3/Al device. Individual presence of PTE derivatives in PVK:PBD host matrix gave yellowish-green electroluminescence with maximum wavelengths of 501 nm, 535 nm, 536 nm, and 545 nm and luminance values (cd/m^2) of 233, 35, 442, and 196 for PTEref, PTE1, PTE2 and PTE3, respectively. Whereas dual doping them produced greenish-white light; luminance (cd/m^2) and EQE (%) values of 570, 1073, 1099 and 0.22, 0.24, 0.26 with the full width of half maximum values (nm) of 76, 109, and 108 for PTEref:PTE1, PTEref:PTE2 and PTEref:PTE3, respectively were obtained. It is thought that the π-π interaction between the PTE cores was minimized by the steric inheritance of PTE3 and this became the dominant effect in reaching high efficiency values with broadened EL without the need of a red emitter contribution. It is projected that further enhancement in the efficiency values of these devices could be reached with the use of suitable electron transfer and/or hole blocking layers.

Author contribution statement

The first and second authors contributed equally to the manuscript. Erkan Aksoy: Conceptualization, methodology, formal analysis and investigation on material synthesis, photophysical and device characterization, writing - original draft. Volkan Bozkus: Methodology, validation, formal analysis and investigation on device characteristics, writing - original draft. Canan Varlikli: Conceptualization, writing - review & editing, supervision, and project administration. All authors have given approval to the final version of the manuscript.

Declaration of competing interest

The authors declare the following financial interests/personal relationships which may be considered as potential competing interests: Canan VARLIKLI reports financial support was provided by Scientific and Technological Research Council of Turkey.

Data availability

The authors do not have permission to share data.

Acknowledgements

Authors are thankful to the project support funds of the Scientific Research Council of Turkey (TUBITAK) (Project Number: 119F031) and undergraduate student Zeynep Saatci who acted as a star scholar in the project.

Appendix A. Supplementary data

Supplementary data to this article can be found online at https://doi.org/10.1016/j.dyepig.2022.111050.

References

[1] Jiang Y, Lu L, Yang M, Zhan C, Xie Z, Verpoort F, et al. Taking the place of perylene diimide: perylene tetracarboxylic tetraester as a building block for polymeric acceptors to achieve higher open circuit voltage in all-polymer bulk heterojunction solar cells. Polym Chem 2013;4:5612–20. https://doi.org/10.1039/c3py00938f.

[2] Bala I, Singh N, Yadav RAK, De J, Gupta SP, Singh DP, et al. Room temperature perylene based columnar liquid crystals as solid-state fluorescent emitters in solution-processable organic light-emitting diodes. J Mater Chem C Mater 2020;8:12485–94. https://doi.org/10.1039/d0tc02754e.

[3] Mosca M, Caruso F, Zambito L, Macaluso R, Cali C, Feltin E. Hybrid LEDs pave way to new lighting applications. Photon Spectra 2013;47:60–4.

[4] Mosca M, Caruso F, Zambito L, Seminara B, Macaluso R, Calì C, et al. Warm white LED light by frequency down-conversion of mixed yellow and red Lumogen. Proc SPIE-Int Soc Opt Eng 2013;8767:87670L. https://doi.org/10.1117/12.2017274.

[5] Caruso F, Mosca M, Macaluso R, Feltin E, Calì C. Generation of white LED light by frequency downconversion using perylene-based dye. Electron Lett 2012;48:1417–9. https://doi.org/10.1049/el.2012.3084.

[6] Galeotti F, Mróz W, Catellani M, Kutrzeba-Kotowska B, Kozma E. Tailorable perylene-loaded fluorescent nanostructures: a multifaceted approach enabling their application in white hybrid LEDs. J Mater Chem C 2016;4:5407–15. https://doi.org/10.1039/C6TC00486E.

[7] Ruetten Sa, Thomas JK. Fluorescence and triplet quantum yields of arenes on surfaces. J Phys Chem B 1998;102:598–606. https://doi.org/10.1021/jp972934o.

[8] Mosca M, Macaluso R, Crupi I. Hybrid inorganic-organic white light emitting diodes. Polymers for Light-Emitting Devices and Displays 2020:197–262. https://doi.org/10.1002/9781119654643.ch8.

[9] Fang H, Xia D, Zhao C, Zhou S, Wang R, Zang Y, et al. Perylene bisimides-based molecular dyads with different alkyl linkers for single-component organic solar cells. Dyes Pigments 2022;203:110355. https://doi.org/10.1016/j.dyepig.2022.110355.

[10] Zheng X, Wei Q, Shan T, Zhang Y, Zhong H. The halogen effect of perylene diimide-based non-fullerene acceptors on photovoltaic properties. Dyes Pigments 2022;201:110232. https://doi.org/10.1016/j.dyepig.2022.110232.

[11] Matussek M, Filapek M, Gancarz P, Krompiec S, Grzegorz Małecki J, Kotowicz S, et al. Synthesis and photophysical properties of new perylene bisimide derivatives for application as emitting materials in OLEDs. Dyes Pigments 2018;159:590–9. https://doi.org/10.1016/j.dyepig.2018.07.006.

[12] Rahmati M, Dayneko SV, Pahlevani M, Welch GC. Interlayer engineering of flexible and large-area red organic-light-emitting diodes based on an n-annulated perylene diimide dimer. ACS Appl Electron Mater 2020;2:48–55. https://doi.org/10.1021/acsaelm.9b00688.

[13] Céspedes-Guirao FJ, García-Santamaría S, Fernández-Lázaro F, Sastre-Santos a, Bolink HJ. Efficient electroluminescence from a perylenediimide fluorophore obtained from a simple solution processed OLED. J Phys D Appl Phys 2009;42:105106. https://doi.org/10.1088/0022-3727/42/10/105106.

[14] Kozma E, Mróz W, Villafiorita-Monteleone F, Galeotti F, Andicsová-Eckstein A, Catellani M, et al. Perylene diimide derivatives as red and deep red-emitters for fully solution processable OLEDs. RSC Adv 2016;6:61175–9. https://doi.org/10.1039/C6RA10467C.

[15] Jiang K, Wu F, Yu H, Yao Y, Zhang G, Zhu L, et al. A perylene diimide-based electron transport layer enabling efficient inverted perovskite solar cells. J Mater Chem A Mater 2018;6:16868–73. https://doi.org/10.1039/c8ta06081a.

[16] Ganesan P, Tsao HN, Gao P. En route to wide area emitting organic light-emitting transistors for intrinsic drive-integrated display applications: a comprehensive review. Adv Funct Mater 2021;31:1–39. https://doi.org/10.1002/adfm.202105506.

[17] Ma Y, Cai D, Wan S, Yin P, Wang P, Lin W, et al. Control over π-πstacking of heteroheptacene-based nonfullerene acceptors for 16% efficiency polymer solar cells. Natl Sci Rev 2020;7:1886–95. https://doi.org/10.1093/nsr/nwaa189.

[18] Giri G, Verploegen E, Mannsfeld SCB, Atahan-Evrenk S, Kim DH, Lee SY, et al. Tuning charge transport in solution-sheared organic semiconductors using lattice strain. Nature 2011;480:504–8. https://doi.org/10.1038/nature10683.

[19] Keum C, Becker D, Archer E, Bock H, Kitzerow H, Gather MC, et al. Organic light-emitting diodes based on a columnar liquid-crystalline perylene emitter. Adv Opt Mater 2020;8. https://doi.org/10.1002/adom.202000414.

[20] Aksoy E, Danos A, Varlikli C, Monkman AP. Navigating CIE space for efficient TADF downconversion WOLEDs. Dyes Pigments 2020;183:108707. https://doi.org/10.1016/j.dyepig.2020.108707.

[21] Guner T, Aksoy E, Demir MM, Varlikli C. Perylene-embedded electrospun PS fibers for white light generation. Dyes Pigments 2019;160:501–8. https://doi.org/10.1016/j.dyepig.2018.08.040.

[22] Bozkus V, Aksoy E, Varlikli C. Perylene based solution processed single layer woled with adjustable CCT and CRI. Electronics (Switzerland) 2021;10:1–12. https://doi.org/10.3390/electronics10060725.

[23] Oner I, Varlikli C, Icli S. The use of a perylenediimide derivative as a dopant in hole transport layer of an organic light emitting device. Appl Surf Sci 2011;257:6089–94. https://doi.org/10.1016/j.apsusc.2011.02.002.

[24] Vollbrecht J, Blazy S, Dierks P, Peurifoy S, Bock H, Kitzerow H. Electroluminescent and optoelectronic properties of OLEDs with bay-extended, distorted perylene esters as emitter materials. ChemPhysChem 2017;18:2024–32. https://doi.org/10.1002/cphc.201700502.

[25] Gupta RK, Das D, Gupta M, Pal SK, Iyer PK, Achalkumar AS. Electroluminescent room temperature columnar liquid crystals based on bay-annulated perylene tetraesters. J Mater Chem C Mater 2017;5:1767–81. https://doi.org/10.1039/c6tc04166c.

[26] Gupta RK, Das D, Iyer PK, Achalkumar AS. First example of white organic electroluminescence utilizing perylene ester imides. ChemistrySelect 2018;3:5123–9. https://doi.org/10.1002/slct.201801258.

[27] Gupta RK, Ulla H, Satyanarayan MN, Sudhakar AA. A perylene-triazine-based star-shaped green light emitter for organic light emitting diodes. 2018 Eur J Org Chem 2018:1608–13. https://doi.org/10.1002/ejoc.201800161.

[28] Dhingra Shallu, Siddiqui Iram, Gupta Santosh Prasad, Shahnawaz, Jayakumar Jayachandran, Jou Jwo-Huei, Pal SK. Solution-processable organic light-emitting diodes utilizing electroluminescent perylene tetraesters-based columnar liquid crystals. Soft Matter 2022. https://doi.org/10.1002/9783527617050. Accepted Manuscript.

[29] Gupta RK, Pathak SK, Pradhan B, Shankar Rao DS, Krishna Prasad S, Achalkumar AS. Self-assembly of luminescent N-annulated perylene tetraesters into fluid columnar phases. Soft Matter 2015;11:3629–36. https://doi.org/10.1039/c5sm00463b.

[30] Ozser ME, Sarkodie Sa, Mohiuddin O, Ozesme G. Novel derivatives of regioisomerically pure 1,7-disubstituted perylene diimide dyes bearing phenoxy and pyrrolidinyl substituents: synthesis, photophysical, thermal, and structural properties. J Lumin 2017;192:414–23. https://doi.org/10.1016/j.jlumin.2017.07.019.

[31] Aksoy E, Danos A, Li C, Monkman AP, Varlikli C. Silylethynyl substitution for preventing aggregate formation in perylene diimides. J Phys Chem C 2021;125:13041–9. https://doi.org/10.1021/acs.jpcc.1c03131.

[32] Murawski C, Leo K, Gather MC. Efficiency roll-off in organic light-emitting diodes. Adv Mater 2013;25:6801–27. https://doi.org/10.1002/adma.201301603.

[33] Wu Z, Ma D. Recent advances in white organic light-emitting diodes. Mater. Sci. Eng. R Rep. 2016;107:1–42. https://doi.org/10.1016/j.mser.2016.06.001.

[34] Kozma E, Kotowski D, Catellani M, Luzzati S, Cavazzini M, Bossi A, et al. Design of perylene diimides for organic solar cell: effect of molecular steric hindrance and extended conjugation. Mater Chem Phys 2015;163:152–60. https://doi.org/10.1016/j.matchemphys.2015.07.025.

[35] Sengupta Sanchita, Dubey Rajeev K., Hoek Rob W.M., van Eeden P., Sjoerd P., Gunbas D. Deniz, et al. Synthesis of regioisomerically pure 1,7-dibromoperylene-3,4,9,10- tetracarboxylic acid derivatives. J. Org. Chem. 2014;79:6655–6662. doi.org/10.1021/jo501180a.

[36] Aksoy E, Demir N, Varlikli C. White LED light production by using dibromoperylene derivatives in down conversion of energy. Can J Phys 2018;96:734–9. https://doi.org/10.1139/cjp-2017-0752.

[37] Wang Q, Liu H, Lu H, Xu Z, Lai G, Li Z, et al. Synthesis, characterization and solid-state emission properties of arylsilyl-substituted pyrene derivatives. Dyes Pigments 2013;99:771–8. https://doi.org/10.1016/j.dyepig.2013.07.003.

[38] Gupta RK, Pathak SK, Pradhan B, Gupta M, Pal SK, Sudhakar AA. Bay-Annulated perylene tetraesters: a new class of discotic liquid crystals. ChemPhysChem 2016;17:859–72. https://doi.org/10.1002/cphc.201501028.

[39] Sebastian E, Philip AM, Benny A, Hariharan M. Null exciton splitting in chromophoric Greek cross (+) aggregate. Angew Chem 2018;130:15922–7. https://doi.org/10.1002/ange.201810209.

[40] Aksoy E, Danos A, Li C, Monkman A, Varlikli C. The effect of imide substituents on the excited state properties of perylene diimide derivatives. Turkish J Sci Technol 2021;33:1209–16. https://doi.org/10.55525/tjst.952823.

[41] Pearce N, Davies ES, Champness NR. Electrochemical and spectroelectrochemical investigations of perylene peri-tetracarbonyl species. Dyes Pigments 2020;183:108735. https://doi.org/10.1016/j.dyepig.2020.108735.

[42] Yan Q, Zhao D. Conjugated dimeric and trimeric perylenediimide oligomers. Org Lett 2009;11:3426–9. https://doi.org/10.1021/ol9012734.

[43] Wen L, Li F, Xie J, Wu C, Zheng Y, Chen D, et al. Electroplex emission at PVK/Bphen interface for application in white organic light-emitting diodes. J Lumin 2011;131:2252–4. https://doi.org/10.1016/j.jlumin.2011.05.056.
[44] Gentili PL. The fuzziness of a chromogenic spirooxazine. Dyes Pigments 2014;110:235–48. https://doi.org/10.1016/j.dyepig.2014.03.024.
[45] Schanda J. International commission on illumination. Colorimetry : understanding the CIE system. 2007. p. 459.
[46] Davis W, Ohno Y. Approaches to color rendering measurement. J Mod Opt 2009;56:1412–9. https://doi.org/10.1080/09500340903023733.
[47] Gentili PL, Rightler AL, Heron BM, Gabbutt CD. Discriminating between the UV-A, UV-B and UV-C regions by novel Biologically Inspired Photochromic Fuzzy Logic (BIPFUL) systems: a detailed comparative study, vol. 135; 2016. p. 169–76. https://doi.org/10.1016/j.dyepig.2016.02.034.